EXPERIMENTAL EVALUATION OF A NATURAL KNEE CONTACT MODEL USING RESPONSE SURFACE OPTIMIZATION

By

YI-CHUNG LIN

A THESIS PRESENTED TO THE GRADUATE SCHOOL
OF THE UNIVERSITY OF FLORIDA IN PARTIAL FULFILLMENT
OF THE REQUIREMENTS FOR THE DEGREE OF
MASTER OF SCIENCE

UNIVERSITY OF FLORIDA

2004

ACKNOWLEDGMENTS

First, I would like to sincerely thank Dr. Benjamin J. Fregly, my advisor, for the direction he has given me throughout my research. His encouragement and dedication have greatly contributed to the accomplishment of this thesis. I would also like to thank Dr. Raphael T. Haftka and Dr. Andrew Kurdila for being my committee members. It was a great honor to have them both.

I would also like to thank all the Computational Biomechanics Lab members for their support in my past and present work, with special thanks to Dong, Yanhong, Jaco and Jeff for their assistance and suggestion.

TABLE OF CONTENTS

Page

LIST OF TABLES

Table page

LIST OF FIGURES

Figure page

Abstract of Thesis Presented to the Graduate School
of the University of Florida in Partial Fulfillment of the
Requirements for the Degree of Master of Science

EXPERIMENTAL EVALUATION OF THE NATURAL KNEE CONTACT MODEL USING RESPONSE SURFACE OPTIMIZATION

By

Yi-Chung Lin

August 2004

Chair: Benjamin Jon Fregly
Major Department: Mechanical and Aerospace Engineering

Finite element, boundary element, and discrete element models have been employed to predict contact conditions in human joints. When optimization is used to evaluate the ability of such models to reproduce experimental measurements, the high computational cost of repeated contact analysis can be a limiting factor. This thesis presents a computationally-efficient response surface optimization methodology to address this limitation. Quadratic response surfaces are fit to contact quantities (peak pressure, average pressure, contact area, and contact force) predicted by a joint contact model for various combinations of material modulus and relative pose (i.e., position and orientation) of the contacting bodies. The response surfaces are used as surrogates for costly contact analyses in an optimization that minimizes differences between measured and predicted contact quantities. The approach is demonstrated by evaluating a linear elastic discrete element contact model of the tibiofemoral joint, where the model was created using CT and MRI data from the same cadaveric specimen used in static pressure

experiments. For variations in material modulus and relative bone pose within the envelope of experimental uncertainty (± 1 mm and 1°), quadratic response surfaces accurately predicted contact quantities computed by the discrete element model. Using these response surfaces, 500 optimizations with different initial guesses were performed in less than 90 seconds. For a flexion angle of 30° and axial loads of 500 and 1000 N, the optimizations demonstrated that small and large strain versions of the contact model could match all experimentally measured contact quantities to within 10% error with the exception of peak contact pressure, which was in error by as much as 85%. Thus, discrete element models of natural joints may be best suited for predicting contact quantities that involve averaging across the surface but not quantities associated with specific locations on the surface.

CHAPTER 1
INTRODUCTION

1.1 Need for Accurate Contact Model

According to the Arthritis Foundation, there were nearly 43 million Americans with arthritis or chronic joint symptoms in 1998. The number went up to 70 million in 2001 and most likely will keep climbing due to the rising number of aging Baby boomers. This foundation also reported that arthritis limits daily activities such as walking, running and dressing for more than seven million Americans. There are many different types of arthritis including osteoarthritis, rheumatoid arthritis, gout, and juvenile arthritis. Among them, osteoarthritis is the most prevalent form of arthritis affecting more than 20.7 million Americans.

Osteoarthritis, or degenerative joint disease, is multifactorial with genetic, biologic, and mechanical factors all playing a role. Of the mechanical factors involved, contact pressure within the joint has been shown to have an interactive effect on developing this disease (Hasler *et al*., 1998; Herzog *et al*., 2003). Thus, knowledge of *in vivo* contact forces and pressures in human joints would be valuable for improving the prevention and treatment of joint arthritis. Although dynamic imaging advances now is capable collecting accurate measurement of *in vivo* joint kinematics (Komistek *et al.*, 2003; Tashman and Anderst, 2003), joint contact forces and pressures are difficult to measure *in vivo* (Kaufman *et al.*, 1996), therefore, necessitating model-based analyses to develop predictions as well as static *in vitro* testing to evaluate these predictions. A variety of joint contact modeling methods have been used for this purpose, including finite element

(Bendjaballah *et al.,* 1995, 1997, 1998; Donzelli and Spilker, 1998; Donahue *et al.,* 2002; Stolk *et al.,* 2002), boundary element (Kuo and Keer, 1993; Haider and Guilak, 2000), and discrete element methods (Li *et al.*, 1999, 2001; Pandy and Sasaki, 1998; Piazza and Delp, 2001; Dhaher and Kahn, 2002).

1.2 Need for Efficient Contact Model Evaluation

Once a joint contact model has been created that represents an *in vitro* testing situation, its ability to reproduce experimentally measured contact quantities (e.g., peak pressure, average pressure, contact area, and contact force) must be evaluated before any further application. At least two factors complicate the process of evaluation. The first is uncertainties in the experimental measurements. These uncertainties can often be estimated and involve quantities such as the position and orientation (i.e., pose) of cadaveric bones measured by the test apparatus, contact pressures and areas recorded by a pressure sensor, and the articular surface geometry determined from medical imaging data. Unknown model parameters, such as material parameters in the contact model, present additional sources of uncertainty.

A second complicating factor is the high computational cost of repeated contact analysis. Given an estimated envelope of uncertainty, optimization methods can be used to determine if a feasible combination of model parameters could be used to reproduce all experimental measurements simultaneously (Fregly *et al*., 2003). For example, an optimization can vary model material parameters and the relative pose of the contacting bodies within the envelope of uncertainty until the model produces the best match to the experimental contact data. The problem with this approach is that the high computational cost of repeated contact analysis can make such optimizations extremely time consuming and in some cases even impractical.

Response surface (RS) methods have been utilized successfully in other situations to eliminate computational bottlenecks in optimization studies. Response surfaces are simply multi-dimensional linear regression curve fits to quantities of interest predicted by an engineering model. Once the mathematical form of the RS is specified, linear least squares is typically used to determine the coefficients that provide the best fit to each predicted quantity of interest (i.e., each response) as a function of the specified design variables. These surface approximations are then used as surrogates for costly engineering analyses when the optimization is performed. Outside of the biomechanics community, RS optimization methods have been used for structural design applications (Jansson *et al*., 2003; Liu *et al*., 2000; Rikards *et al*., 2004; Roux *et al*., 1998), aerodynamic designs (Ahn and Kim, 2003; Papila *et al*., 2002; Sevant *et al*., 2000), and fluid dynamics (Burman and Gebart, 2001; Keane, 2003; Leary *et al*., 2004). Within the biomechanics community, little work has been performed using RS optimization methods with the exception of recent studies by Jung and Choe (1996), Chang *et al*. (1999), and Hong *et al.* (2001). To our knowledge, no studies in the literature have used RS methods to perform optimizations of contact problems.

1.3 Approach

The two goals of this thesis are first, to develop a computationally efficient RS optimization approach for evaluating a joint contact model's ability to reproduce static experimental contact measurements, and second, to apply this approach to the evaluation of a discrete element contact model of the tibiofemoral joint. Our specific hypotheses were that 1) quadratic RSs can accurately predict contact quantities (peak pressure, average pressure, contact area, and contact forces) computed by a discrete element contact model for small variations material modulus and relative pose of the contacting

bodies, and 2) a discrete element contact model of the tibiofemoral joint can reproduce experimentally measured contact quantities that involve averaging across the surface (i.e., average pressure, contact area, contact force) but not quantities associated with specific locations on the surface (i.e., peak pressure). Our study provides a new computationally-efficient approach for contact model evaluation as well as a better understanding of the capabilities and limitations of discrete element contact models of natural human joints.

CHAPTER 2
METHODS

2.1 Response Surface Optimization

This section provides a general overview of RS approximation methods as well as specific modifications required to apply these methods to contact analyses. The RS method can be defined as a collection of statistical and mathematical techniques useful for constructing smooth approximations to functions in a multi-dimensional design space. Once a mathematical form has been selected, the coefficients of the approximate function (responses surface) are determined using data from either physical experiments or numerical simulations. The most common mathematical form for a RS is a low-degree polynomial. For example, a quadratic response surface with design variable inputs x_1 and x_2 and output y is formulated as

$$y = \beta_0 + \beta_1 x_1 + \beta_2 x_2 + \beta_3 x_1^2 + \beta_4 x_2^2 + \beta_5 x_1 x_2 \tag{1}$$

where the β_i ($i = 0,\ldots,5$) are the unknown coefficients to be fitted. A low degree polynomial minimizes the number of unknown coefficients and tends to smooth out noise in the function. Response surface approximations work best when the number of design variable inputs is small (< 10), since a large number of design variables results in a complicated design space that is difficult to fit with low-degree polynomials

To develop RS approximations for contact problems, one must identify the design variable (DV) inputs, the outputs to be predicted, and the mathematical form of the RS relating them. For contact model evaluation with static experimental data, the design

variables are the six relative pose parameters (i.e., three translations and three rotations - 6 DVs) and material modulus (1 DV) of the contacting bodies. The experimental uncertainty of these quantities can be estimated and their values can be changed in the contact model. The RS outputs are peak pressure, average pressure, contact area, and contact force. These quantities can be calculated by the contact model and measured experimentally for comparison. The hypothesized mathematical form is a quadratic RS with one modification. For linearly elastic Hertzian point contact, the peak pressure, average pressure, contact force, and contact area are all functions of interpenetration (vertical translation) to a power less than two, while the material modulus (assumed to be the same for both bodies) linearly scales each quantity except for area (Johnson, 1985). Thus, data for the RSs are generated using a material modulus of one, only the six pose parameters are used as RS inputs, and the RS outputs (except area) are scaled by the desired modulus value.

With the RS formulation specified, the next step is to determine a sampling scheme within the design space to provide data for fitting the RS. Since this sampling process is only preformed once to generate the RSs, the computational cost of the contact analyses is paid only once up front. A quadratic response surface using k design variables will possess $p = (k+1)(k+2)/2$ unknown coefficients, where $k = 6$ since only pose parameters are used as RS inputs. Consequently, a minimum of $p = 28$ data points must be sampled to perform the linear least-squares fit. However, to cover the design space in a systematic manner, we select a larger number of sample points using design of experiments (DOE) theory. Several DOE sample criteria are available, including the factorial design, face centered central composite design (FCCCD), and the D-optimality

design. We choose the FCCCD criteria for its ability to sample all regions of the design space. For a quadratic RS, this approach utilizes $2^k + 2k + 1 = 77$ sample points, where the samples are taken at the center, the corners, and the face centers of a *k* dimensional hypercube.

For contact analyses, we make two modifications to the FCCCD sampling scheme to improve the quality of the fit. The first modification accounts for infeasible points. A sampled point is deemed to be infeasible and is therefore omitted if the contact force and area predicted by the contact model are zero. This modification avoids fitting regions of the design space where no contact is occurring. The second modification accounts for outlier points. Once a RS is generated from feasible points, the RS output is compared to the computed value from the contact model for every sample point. The point with the largest absolute percent error above a pre-selected cut-off value of 10% (a typical value for engineering analyses) is omitted and the RS re-generated from the remaining sample points. The procedure is iterated until all sample points are below 10% error. This modification avoids fitting regions of the design space where only light contact is occurring, thereby providing a better fit in the regions of interest where the contact force is large. Omission of several sample points does not pose a problem to the fitting process since the FCCCD sampling scheme is highly over determined.

After a RS is generated, the quality of the resulting fit must be assessed, since a poor quality fit indicates that a different mathematical form for the RS should be considered. We use three common error measures for this purpose. All of these measures make use of the sum of the squares of the errors *SSE* between predicted responses $\hat{y}_i$ from

the RS and actual responses y_i computed by the contact model, where n ($n >> 28$ and $n \leq 77$) is the number of sample points used to generate the RS:

$$SSE = \sum_{i=1}^{n} (y_i - \hat{y}_i)^2 \tag{2}$$

The first measure of fit quality is the adjusted root-mean-square error ($RMSE_{adj}$). Given the *SSE*, the root-mean square error (*RMSE*) can be calculated from

$$RMSE = \sqrt{\frac{SSE}{n}} \tag{3}$$

However, this measure will be zero if $n = p$ (i.e., no redundant points), even though the errors would not necessarily be zero at non-sampled points. To address this limitation, we choose a more conservative adjusted *RMSE* that uses $n - p$ (i.e., the number of degrees of freedom remaining in the fitting process) rather than n in the denominator of Eq. (3):

$$RMSE_{adj} = \sqrt{\frac{SSE}{n - p}} \tag{4}$$

To provide a relative measure of fit quality, we also compute the percent adjusted *RMSE* using

$$\%RMSE_{adj} = \frac{100}{\tilde{y}} \sqrt{\frac{SSE}{n - p}} \tag{5}$$

where $\tilde{y}$ represents the magnitude of the fitted quantity:

$$\tilde{y} = \frac{1}{n} \sum_{i=1}^{n} |y_i| \tag{6}$$

The second measure of fit quality is the adjusted coefficient of determination ($R^2{}_{adj}$). The coefficient of determination R^2 suffers from a similar problem to RMSE in

that a perfect fit will be indicated if $n = p$. Consequently, we used the adjusted R^2 value to account for the degrees of freedom $n - p$ remaining in the fit:

$$R^2_{adj} = 1 - \frac{SSE/(n-p)}{\sum_{i=1}^{n}(y_i - \bar{y})^2/(n-1)} \tag{7}$$

where $\bar{y}$ is the mean of the actual responses.

The final measure of fit quality is the *RMSE* calculated from the prediction error sum of squares (*PRESS*) statistic. To evaluate the predictive capability of a RS, one should ideally sample additional points distinct from those used to generate the RS. However, this approach would require a significant number of additional costly contact analyses. To circumvent this issue, the *PRESS* analysis excludes one sample point at a time from the set used to generate each RS. The RS is regenerated using the remaining $n-1$ sample points and the prediction error at the omitted sample point calculated. This process is repeated for all *n* sample points, and the resulting errors are used to compute a *PRESS*-based *SSE* called the *PRESS* statistic. From there, a *PRESS*-based *RMSE* can be calculated from Eq. (3), where n rather than $n - p$ is used in the denominator since each error is calculated from a RS that omits that point.

Once accurate RSs are generated for the output quantities of interest, they are used in an optimization to evaluate the contact model's ability to reproduce experimental measurements. Each time the optimization requires a peak pressure, average pressure, contact force, or contact area from the contact model, a response surface is used in place of a contact analysis to provide the value. By fitting quantities computed by the contact model, one can create any cost function that can be built up from the basic quantities. If the cost function was fitted directly using its own response surface, then additional

contact analyses would be required to generate a new response surface each time the cost function was modified. With our approach, a wide variety of cost functions can be constructed without the need for any additional contact analyses.

2.2 Contact Pressure Experiments

The response surface methodology described above was used to evaluate a natural knee contact model's ability to reproduce experimental contact measurements. The experiments were performed on a single cadaveric knee specimen cut approximately 15 cm above and below the joint line and showing no visible signs of degenerative joint disease. Institutional review board approval was obtained for the testing and subsequent modeling efforts. The menisci, fibula, and patella were removed from the specimen, and three titanium bone screws were inserted into the tibia and femur as landmarks for contact model alignment. The tibia and femur were potted in neutral alignment (MacWillams *et al*., 1998) and mounted in a MTS MiniBionix 858 servohydraulic test machine. The position and orientation of the femur were constrained using custom fixturing that allowed adjustment of the sagittal plane rotation and medial-lateral translation relative to the ram of the test machine. The axial plane position and orientation of the tibia were unconstrained using a ball plate, thereby allowing the tibia to self-align with the femur once an axial load was applied.

Using this set-up (Fig. 2-1), we collected four experimental quantities of interest from the medial and lateral compartments of the knee: contact force, peak pressure, average pressure, and contact area. The knee was fixed at a flexion angle of 30º and a Tekscan K-scan sensor (Tekscan, South Boston, MA) inserted anteriorly into the medial and lateral joint space. The medial-lateral position of the femur was adjusted to produce an approximately 70% medial-30% lateral load split between the two sides (Hurwitz *et*

al., 1998; Schipplein and Andriacchi, 1991). The specimen was subjected to three trials of a 4 second ramp load from 200 to 1000 N. At the end of each ramp, the locations of the six screw heads were digitized using a Microscribe 3DX digitizer (Immersion Corp., San Jose, CA) possessing an accuracy of 0.23 mm.

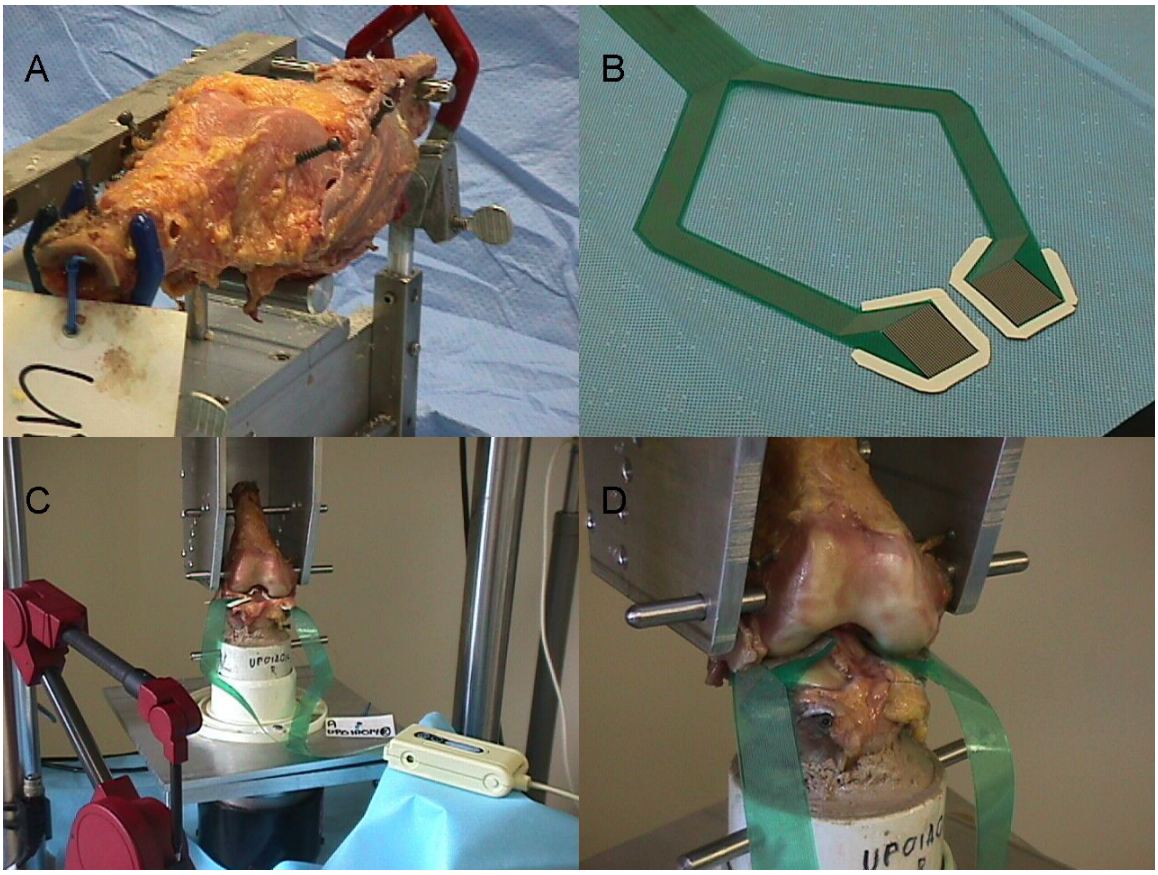

Figure 2-1. A human cadaver knee static experiment setup. A) The knee was potted in neutral alignment with six screws. B) The Tekscan K-scan sensor. C) The knee was mounted with fixed 30^{o} flexion angle in a servohydraulic test machine with a sensor to measure intra-articular contact quantities. D) The close-up view of the contact area.

Drift in the Tekscan sensor (Otto *et al.*, 1999) was eliminated by post-calibrating each trial with the manufacturer-suggested two-point calibration procedure using the known loads at the start and end of the ramp. Crinkling of the sensor (Harris *et al.*, 1999), which introduces erroneous pressures on sensels outside the true contact area, was accounted for by determining the pressure cut-off value (0.05 MPa) above which little

additional drop in contact area occurs when pressures below this value are set to zero (Fregly *et al*., 2003). Contact quantities measured with the Tekscan sensor were therefore calculated by ignoring all sensels with a pressure below 0.05 MPa. Following Tekscan sensor calibration and pressure cut-off determination, the four experimental quantities of interest were calculated on each side for applied loads of 500 and 1000 N. Peak pressure was calculated using the averaging function in the Tekscan software, thereby reducing the effect of local sensor "hot spots" on this quantity. The resulting data from the K-scan sensor (Table 2-1) and the digitizer were averaged over the three trials to facilitate contact model evaluation under two loading conditions.

Table 2-1. The averaged experimental measurements were collected from three compression trials for both loads processing on the same cadaver knee via servohydraulic test machine

		Experimental Load	
Experimental Quantity	**Side**	**500 N**	**1000 N**
Force (N)	Medial	317 ± 4	658 ± 5
Max Pressure (MPa)		4.10 ± 0.05	7.94 ± 0.14
Ave Pressure (MPa)		1.11 ± 0.03	2.07 ± 0.02
Area (mm^2)		287 ± 10	318 ± 4
Force (N)	Lateral	183 ± 4	337 ± 5
Max Pressure (MPa)		1.51 ± 0.03	2.63 ± 0.04
Ave Pressure (MPa)		0.79 ± 0.01	1.33 ± 0.03
Area (mm^2)		229 ± 4	252 ± 5

2.3 Knee Model Creation

Prior to experimental contact testing, MRI (magnetic resonance imaging) and CT (computed tomography) data were collected from the same cadaveric specimen for purposes of contact model creation. Sagittal plane MRI data were collected using a 3.0-T GE Signa Horizon LX scanner with a quadrature knee coil. A T2-weighted 3D FastGRE sequence was used with a 1 mm slice thickness, 256 x 256 image matrix (0.625 × 0.625

mm pixel size), and 160 x 160 mm field of view. Axial CT data were collected from the same specimen using a GE LightSpeed QX/i scanner in helical mode. The scanning parameters were a 1.25 mm overlapping slice thickness, 512 x 512 image matrix (0.313 × 0.313 mm pixel size), and 160 mm x 160 mm field of view. The tibia, femur, and bone screws in both data sets were segmented (Fig. 2-2) using commercial image processing software (SliceOmatic, Tomovision, Montreal, CA).

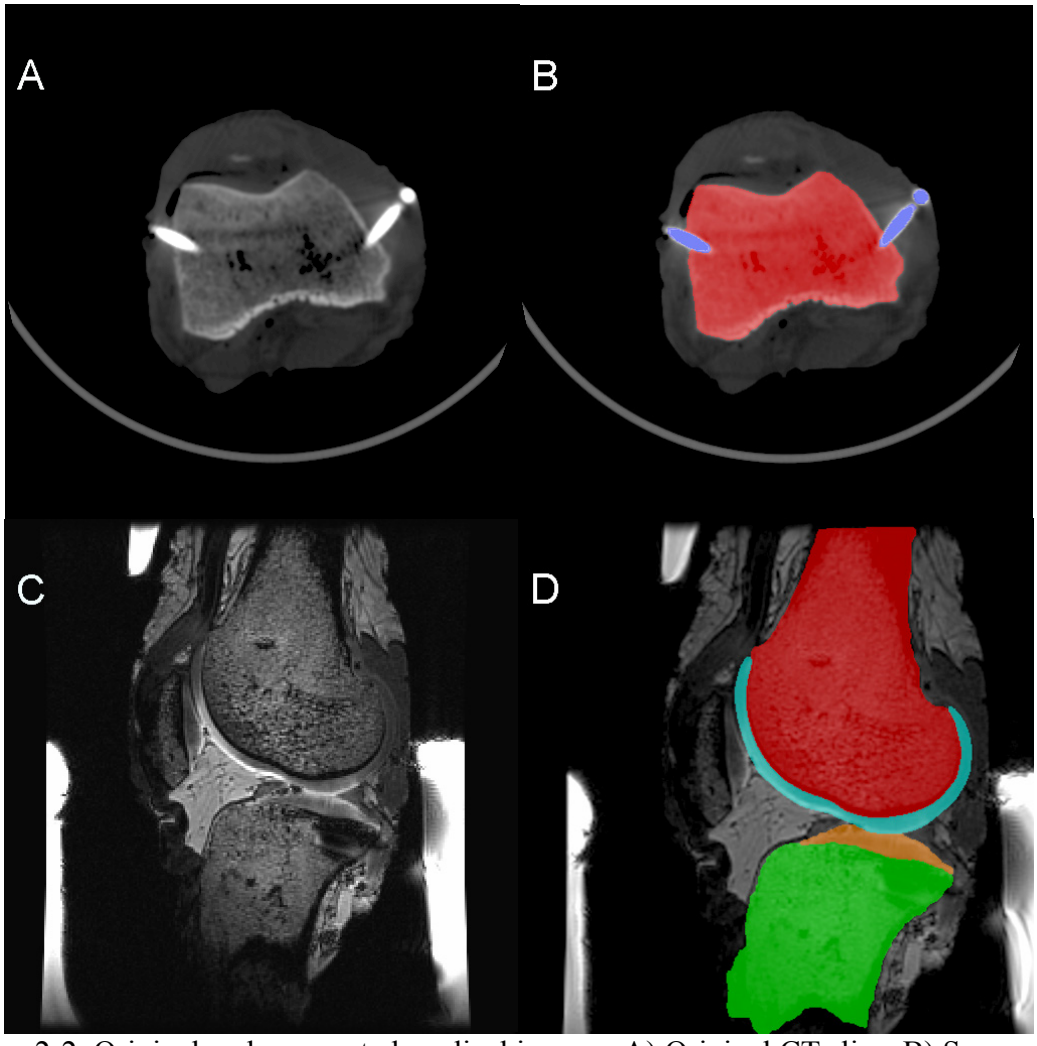

Figure 2-2. Original and segmented medical images. A) Original CT slice. B) Segmented CT slice. C) Original MRI slice. D) Segmented MRI slice.

The menisci were not segmented and were omitted from the model. Articular cartilage and subchondral bone surfaces were segmented manually from the MRI data,

while cortical bone and bone screw surfaces were segmented semi-automatically from the CT data using a watershed algorithm. The point clouds from both scans were exported for subsequent surface creation.

Commercial reverse engineering software (Geomagic Studio, Raindrop Geomagic, Research Triangle Park, NC) was used to convert the MRI and CT point cloud data into a combined geometric model for contact analysis. Point clouds from each imaging modality were imported separately and converted to polygonal surface models. The subchondral bone surfaces from MRI were registered automatically to the corresponding cortical bone surfaces from CT, creating a composite geometric model with articular cartilage surfaces from MRI and cortical bone and bone screw surfaces from CT. NURBS (Non-Uniform Rational B-Spline) surfaces were fitted to the polygonal models, with the tolerance (mean ± standard deviation) between the original point clouds from MRI and the final NURBS surfaces being 0.18 ± 0.18 mm for the femur and 0.20 ± 0.29 mm for the tibia (Fig. 2-3).

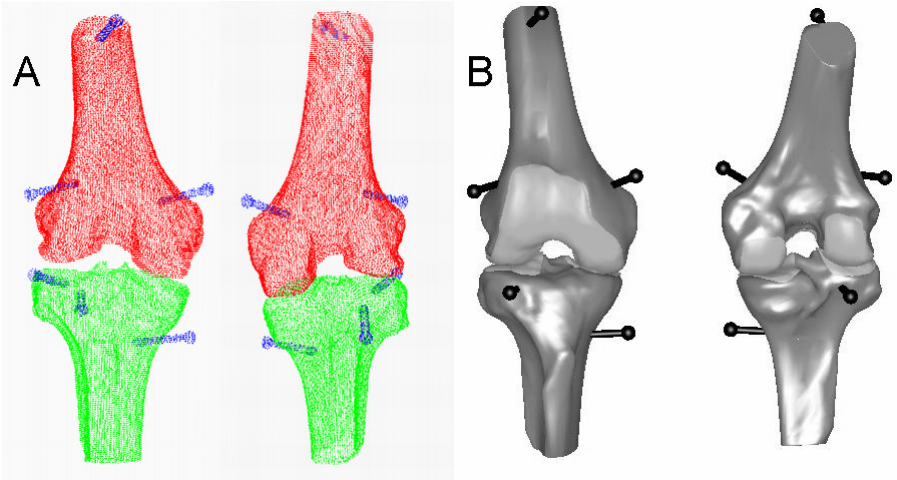

Figure 2-3. The anterior and posterior views of the A) 3D point clouds and B) 3D NURBS model with six screws created from CT and MRI images

The NURBS surfaces for the tibia and femur (articular cartilage, cortical bone, and bone screws) were imported into Pro/MECHANICA MOTION (Parametric Technology

Corporation, Waltham, MA) to construct a multibody contact model. The mean digitized bone screw locations were also imported to determine the nominal alignment of the tibia and femur. For both bones, a stiff linear spring was placed between each screw head and its mean experimental location and a static analysis performed to determine the pose that best matched the experiments. Differences between the digitized and nominal bone screw locations were on the order of 1 mm. Starting from these nominal poses, the tibia was fixed to ground and the femur connected to it via a 6 degree-of-freedom (DOF) joint.

Custom contact code was incorporated into the multibody model and used to solve for the medial and lateral contact conditions as a function of the 6 DOFs between the two bones (Bei and Fregly, 2004). The contact code implemented two versions of a linear elastic discrete element contact model. The first was a small strain version, where the contact pressure p for each contact element on the tibial articular surfaces was calculated from (An *et al.*, 1990; Blankevoort *et al*., 1991; Li *et al.,* 1997)

$$p = \frac{(1-\nu)E}{(1+\nu)(1-2\nu)}\frac{d}{h} \tag{8}$$

where E is Young's modulus of the articular cartilage, ν is Poisson's ratio, h is the combined thickness of the femoral and tibial articular cartilage, and d is the interpenetration of the undeformed contact surfaces. Both h and d were calculated on an element-by-element basis using the ACIS 3D Toolkit (Spatial Corporation, Wesminster, CO). For large strains, a second version of the model was implemented that accounted for geometric nonlinear behavior (Blankevoort *et al*., 1991):

$$p = \frac{-(1-\nu)E}{(1+\nu)(1-2\nu)}\ln\left[1-\frac{d}{h}\right] \tag{9}$$

For both versions, a dense contact element grid of 50 x 50 was used for the medial and laterial articular surfaces of the tibia. The femoral and tibial articular cartilage were assumed to be linear elastic and isotropic with Poisson's ratio = 0.45 (Blankevoort *et al.*, 1991). Young's modulus was set to 1 MPa to facilitate its use as a design variable in the response surface optimizations.

2.4 Knee Model Evaluation

Seventy seven contact analyses were performed with the model to provide the sample points necessary to generate response surfaces using the FCCCD. Each sample point represented a different pose of the femur relative to the tibia within the neighborhood of the nominal pose. This neighborhood was defined to be ± 1 mm and ± 1° based on the estimated envelope of experimental pose uncertainty. Though this envelope appears small, it corresponds to large changes in contact conditions. Within this envelope, response surfaces were generated as described above for the medial and lateral contact force, peak pressure, average pressure, and contact area computed by the contact model. The optimization cost function $g(\mathbf{x})$ constructed from these response surfaces sought to match experimental average pressures p_{ave} in both compartments simultaneously with a penalty term to ensure the experimental contact forces *F* were reproduced:

$$g(\mathbf{x},E) = (p_{ave} - E\,\hat{p}_{ave}(\mathbf{x}))^2_{medial} + (p_{ave} - E\,\hat{p}_{ave}(\mathbf{x}))^2_{lateral} + w\left[(F - E\hat{F}(\mathbf{x}))^2_{medial} + (F - E\hat{F}(\mathbf{x}))^2_{lateral}\right] \tag{10}$$

where $\hat{F}(\mathbf{x})$ and $\hat{p}_{ave}(\mathbf{x})$ are the force and average pressure predicted by response surfaces.

In this equation, **x** represents the 6 pose parameter design variables, E is the material modulus seventh design variable, and $w = 1000$ is the weight of the penalty term. This cost function mimics the results of a static analysis, since contact force is matched closely while minimizing errors in the most reliable experimental measure of interest. The form of Eq. (10) was specified by following a trial-and-error approach that included different quantities in the cost function. A larger value of w was not used since it resulted in a poor match to the other contact quantities.

To seek the global minimum, we performed 500 nonlinear least-squares optimizations using the response surfaces from each contact model and the Matlab Optimization Toolbox (The Mathworks, Natick, MA). Uniformly distributed random initial guesses were selected within the bounds ± 1 for the first six design variables and 1 to 10 for the seventh. The best set of design variables was selected based on the smallest cost function value from the 500 optimizations. A final Pro/MECHANICA contact analysis was performed for both contact models using the optimized design variables to verify the accuracy of the response surface approximations.

CHAPTER 3
RESULTS

All $\%RMSE_{adj}$ and $\%RMSE_{press}$ results were less than 5% while all $R^2{}_{adj}$ values were greater than or equal to 0.995. Error measures from the small and large strain versions of the contact model were generally close. $\%RMSE_{press}$ was always larger than $\%RMSE_{adj}$ but not dramatically so. Furthermore, $\%RMSE_{adj}$ and $\%RMSE_{press}$ were of comparable magnitude to the variability in the corresponding experimental measurements (Table 3-1). For each RS, a minimum of 7 and maximum of 26 infeasible/outlier points were eliminated from the original FCCCD set of 77 sample points, and all of these points involved a superior translation of +1 mm (i.e., no contact or light contact).

Based on the best results from the 500 RS optimizations, the contact quantities computed from response surfaces were compared to both versions of the contact model (Fig. 3-1). The relative errors from all contact quantities were below 10%. Both versions of the contact model could reproduce all experimentally measured contact quantities to within 10% error at both loads (Fig. 3-2). The one exception was peak pressure, which was only matched to within 50% error. Contact force was matched to within 1% error, consistent with the use of a penalty term on this quantity in the cost function. Average pressure and contact area errors were always in opposite directions, consistent with matching contact force closely. Peak pressure was over-predicted by the contact models on the lateral side and under-predicted on the medial side (worst error). The optimal value of Young's modulus was 2.6 MPa for the small strain model and 2.3 MPa for the

large strain one. The best result from 500 optimizations never hit the upper or lower bounds on the pose parameter design variables. Each set of 500 optimizations required approximately 90 seconds of CPU time on a 2.8 GHz Pentium 4 PC.

Table 3-1. Comparison of response surface predictions to data points sampled from large and small strain contact models.

		$RMSE_{adj}$		$\%RMSE_{adj}$		$RMSE_{press}$		$\%RMSE_{press}$		R^2_{adj}	
Predicted Quantity	**Side**	Large	Small	Large	Small	Large	Small	Large	Small	Large	Small
Force (N)	Medial	4.67	4.24	0.601	0.674	10.0	6.13	1.29	0.976	0.999	0.999
Max Pressure (MPa)		0.065	0.035	1.53	1.16	0.090	0.048	2.13	1.58	0.999	0.999
Ave Pressure (MPa)		0.059	0.048	3.31	3.19	0.078	0.064	4.40	4.25	0.999	0.999
Area (mm^2)		10.8	10.8	3.50	3.50	14.3	14.3	4.64	4.64	0.995	0.995
Force (N)	Lateral	2.12	2.12	0.788	0.886	2.92	2.85	1.09	1.19	0.999	0.999
Max Pressure (MPa)		0.030	0.018	1.15	0.815	0.039	0.023	1.49	1.06	0.999	0.999
Ave Pressure (MPa)		0.026	0.024	2.24	2.27	0.033	0.030	2.91	2.97	0.998	0.998
Area (mm^2)		4.54	4.54	2.58	2.58	6.00	6.00	3.41	3.41	0.996	0.996

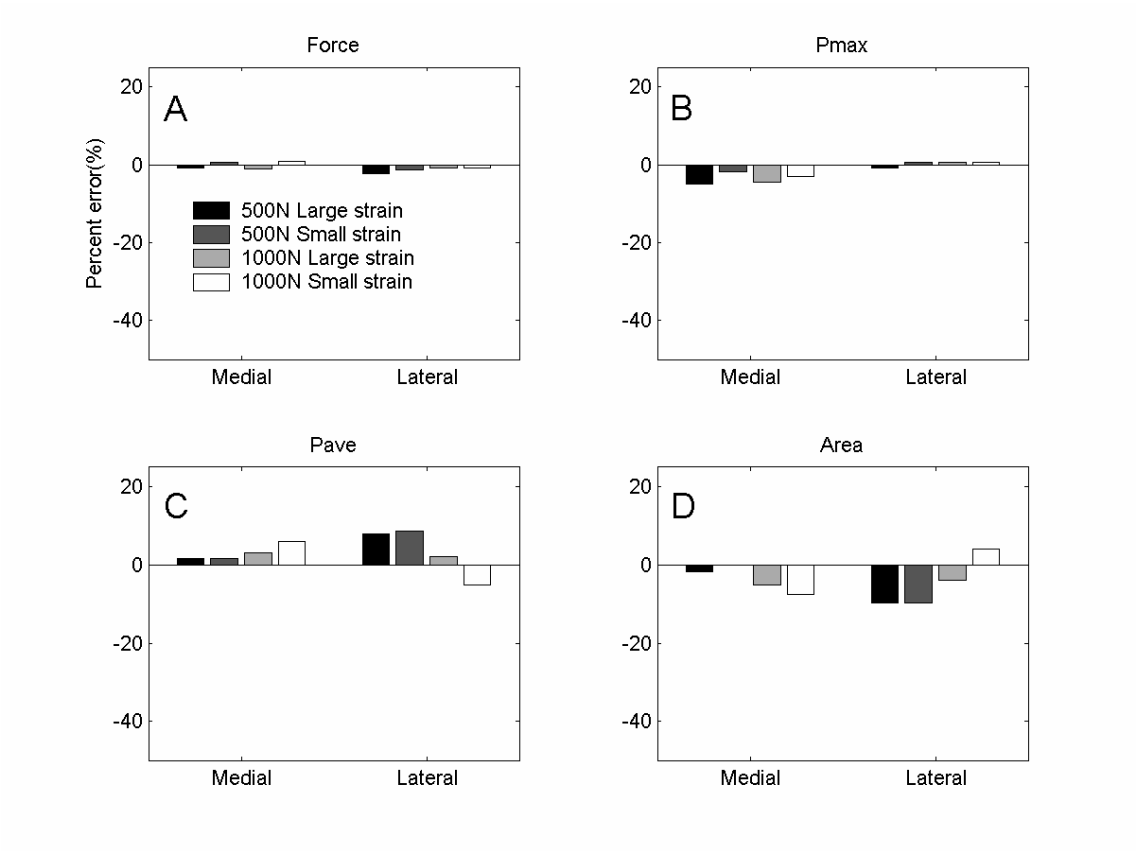

Figure 3-1. Percent errors between response surfaces and predicted results from both contact models. They were calculated for A) contact force, B) contact peak pressure, C) contact averaged pressure and D) contact area. Pose parameters and Young's modulus were defined based on the best result from 500 optimization runs.

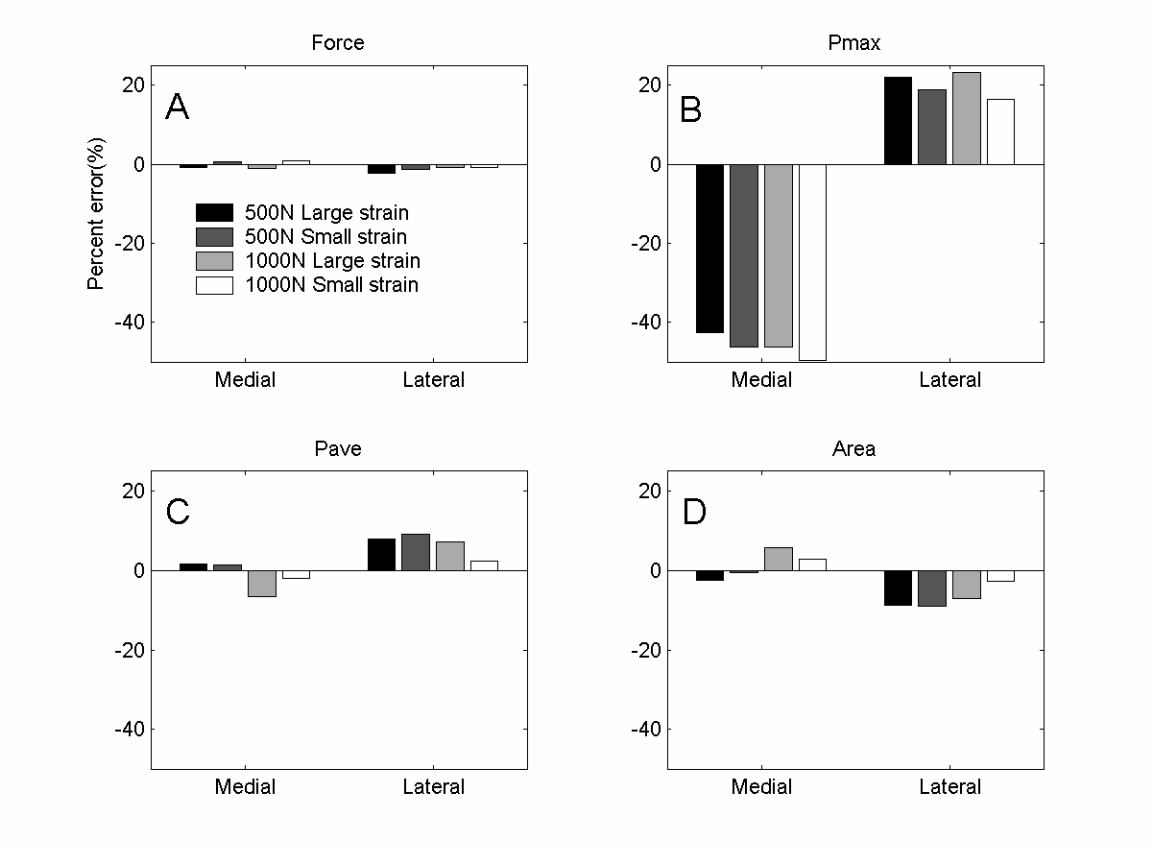

Figure 3-2. Percent errors between experimental and predicted results from both contact models. They were calculated for A) contact force, B) contact peak pressure, C) contact averaged pressure and D) contact area. Pose parameters and Young's modulus were defined based on the best result from 500 optimization runs.

CHAPTER 4
DISCUSSION

This thesis has presented a novel response surface optimization methodology for evaluating a joint contact model's ability to reproduce static experimental contact measurements. The approach modifies traditional RS approximation methods for application to contact analyses. By replacing computationally-costly contact analyses with quadratic RS approximations, optimizations that vary the relative pose of the contacting bodies can be performed rapidly to minimize differences between model predictions and experimental measurements. Evaluation of a discrete element contact model of the tibiofemoral joint constructed from CT and MRI data revealed that quadratic RSs can accurately approximate model outputs within a small envelope of relative pose uncertainty. Furthermore, optimization studies utilizing these RSs demonstrated that the model could reproduce the contact force, average pressure, and contact area. However, the peak pressure measured experimentally on the medial and lateral sides could not be reproduced. This finding suggests that discrete element contact models of natural human joints that utilize homogeneous, isotropic material properties may be best suited for analyses such as multibody dynamic simulations where obtaining correct contact forces by integrating over the surfaces is more critical than obtaining correct contact pressures at specific locations on the surfaces.

Use of RSs to replace repeated contact analyses in optimization studies is worthwhile for several reasons. First, RS tends to smooth out noise in the design space. During optimization, the risk of entrapment in a local minimum is therefore reduced.

Second, RS approximations are computationally efficient. Rather then repeating costly contact analyses during an optimization, a single set of contact analyses is performed once up front to generate the necessary RS approximations for output quantities of interest. Extremely fast function evaluations allow one to search for the global optimum using either repeated gradient-based optimization starting from multiple initial guesses, as performed in our study, or global optimization employing a large population size. Third, RS optimizations are convenient to implement. Optimized contact solutions can be founded utilizing any off-the-shelf optimization algorithm once the RS approximations are constructed. Fourth, a variety of optimization problem formulations can be evaluated quickly. Each contact quantity that could potentially appear in the cost function or constraints can be fitted with its own RS. A wide variety of cost functions can then be constructed by weighting contributions from the different RSs. Fifth, RS approximations facilitate the calculation of analytical derivatives for gradient-based optimization. This benefit is the direct result of having analytical representations for the contact quantities of interest as a function of the design variables. The caveat to these benefits is that an appropriate mathematical form (polynomial or otherwise) must be identified to represent the responses of interest as a function of the design variable inputs, which is not always possible.

The primary deficiency of the discrete element contact model was its inability to match the peak contact pressures measured experimentally. Peak pressures were not included in the cost function since they are sensitive to local inhomogeneities in cartilage material properties and Tekscan sensor response. When we replaced average pressures with peak pressures in the cost function for curiosity, we found that peak pressure errors

decreased on the medial side by about 25% but increased on the lateral side by roughly 50%, while average pressure and contact area errors increased by approximately 30% and 20%, respectively. Thus, a variety of other factors likely contributed to the large peak pressure errors, including insertion of a relatively stiff sensor into the joint space (Wu *et al*., 1998), small inaccuracies in the surface geometry, and local variations in material properties. Underprediction of peak pressure by the model on the moderately conformal medial side and overprediction on the non-conformal lateral side is consistent with observations made by Wu *et al*. (1998) on how insertion of a relatively stiff sensor into the joint space affects peak pressure measurements as a function of contact conformity.

Contact model limitations may have also contributed to the poor match of the peak pressure data. Though a strength of our model is that it accounts for local variations in cartilage thickness, a weakness is that it does not account for local variations in cartilage material properties. Though homogeneous, isotropic cartilage material models have been used in the literature (Bendjaballah *et al*., 1995; Blankevoort *et al*., 1991; Haut *et al*., 2002; Périé and Hobatho, 1998), recent studies have reported significant local variations in Young's modulus, Poisson's ratio and thickness for articular cartilage (Jurvelin *et al*., 2000; Laasanen *et al*., 2003). Mukherjee and Wayne (1998) suggested that regions with the highest Young's modulus correspond to regions with the highest contact pressure and cartilage thickness. This observation fits our under-prediction of peak pressure on the medial side, where an increase in Young's modulus would produce improved agreement with the large measured peak pressures. In addition, our elastic contact model does not account for the effect of time-dependent fluid flow on contact pressures or areas as captured by biphasic models of cartilage (Han *et al*., 2004; Mow *et*

al., 1980; Mow *et al*., 1982). However, for loading over a short time period, an elastic model may still provide a reasonable approximation of the *in vivo* situation depending on the intended application of the model (Donzelli *et al*., 1999; Mow *et al*., 1982; Shepherd and Seedhom, 1997;).

The value of Young's modulus predicted by our optimizations is consistent with studies found in the literature. Experimental studies of the compressive modulus of articular cartilage have reported values as low as 2.0 MPa for short time frame loading (Setton *et al*., 1999; Shepherd and Seedhom, 1997). Other studies have reported the modulus of the solid phase alone to be in the neighborhood of 0.3 MPa (Hasler *et al*., 1999). Thus, the best-fit modulus values of 2.3 and 2.6 MPa found in our study are consistent with these numbers. Other discrete element knee studies have utilized an elastic modulus of 4 MPa (Cohen *et al*., 2003; Kwak *et al*., 2000) which again is close to our optimized modulus values. Furthermore, if our estimate of Poisson's ratio is decreased slightly from 0.45 to 0.4, our optimized value of Young's modulus will increase from 2.6 to 4.6 MPa, closer to the middle of the range commonly reported (Setton *et al*., 1999; Shephard and Seedhom, 1997).

A weakness of our study is that only a single knee specimen was evaluated. Significant modeling effort is required to create a knee model with articular cartilage and subchondral bone geometry that matches a particlar cadaver specimen. This may explain why other studies that utilized specimen-specific geometric models only analyzed a single specimen as well (Bendjaballah *et al*., 1995; Haut *et al*., 2002; Li *et al*., 1999). The knee used in our study was part of a larger experimental study involving 20 knees. However, we were able to collect CT and MRI data from only two of those knees. Since

the contact area for the second specimen was not completely contained within the boundary of the Tekscan sensor at the maximum load of 1000 N, we were not able to post-calibrate those experimental contact data and use them for a second model evaluation. Comparison of model predictions with experimental measurements from additional knee specimens using a range of flexion angles and loads would provide further verification of the capabilities and limitations of discrete element models of natural joints.

CHAPTER 5
SUMMARY AND FUTURE STUDY

5.1 Summary

In summary, this thesis has presented a computationally efficient RS optimization for predicting knee contact measurements using a 3D simulation model. The more computational costly is each contact analysis; the more beneficial is the use of RS optimization method. The present implementation works for the tibiofemoral joint of the natural knee with either large or small strain contact model. The RS optimization can predict contact forces, areas and average pressures well with the exception of peak pressures. Our ultimate goal is to incorporate the elastic foundation contact model into a full-body dynamic musculoskeletal model. The resulting full-body model can then be utilized to study joint contact pressures during motion. Future research is required to evaluate whether the peak pressure errors are due to experimental or contact model inaccuracies.

5.2 Future Study

While our results showed great potential to predict contact quantities that involve averaging across the surface, there are some extra steps that could be taken to improve the accuracy of RS. Instead of using two modifications in this thesis to remove the outliers ,there is another more robust procedure called iteratively re-weighted least square (IRLS) fitting (Holland and Welsch, 1977). It can be utilized to remove or weight down outliers. Additionally, varying numbers of insignificant coefficients for each RS was found based on t-statistics analysis. While it was not performed in this study, there are

several statistical methods, (e.g., a stepwise regression procedure) that can be used to discard those insignificant coefficients to improve the prediction accuracy.

In addition to 500 optimizations, another 50 groups of optimizations were run. The best result was selected from each group containing 100 optimizations with different initial guesses. Within 50 sets of optimized design variables, the maximum variations in translation and rotation were 1.90 mm and 1.95° respectively. Compared to the range of design space, these variations suggested that the final result from 500 optimizations may not be unique. Thus an alternative cost function or type of different RS method (e.g., neural networks and kriging) could be another candidate for future improvement.

Given how well RSs could approximate contact model outputs for a small range of relative pose variations, our next step will be to investigate whether RSs can be used to generate extremely fast forward dynamic contact simulations that utilize a wider range of relative pose variations. The computational cost of repeated geometry evaluations is the current limiting factor to the incorporation of deformable contact models into multibody dynamic simulations of human joints (Bei and Fregly, 2004). However, if accurate response surfaces could be generated to represent the net force and torque calculated about a pre-selected point on the tibia (e.g., the origin of the tibial coordinate system), then extremely fast contact solutions could be produced for any given set of relative pose parameters. Though additional design variables would need to be included to account for friction or damping effects, these effects are expected to be small for most modeling situations involving human joints. Higher degree polynomials or some other mathematical formulation would likely be required to represent a wider range of relative pose variations.

LIST OF REFERENCES

Ahn, C.-S. & Kim, K.-Y. (2003). Aerodynamic design optimization of a compressor rotor with Navier-Stokes analysis. *Proceedings of the Institution of Mechanical Engineers, Part A: Journal of Power and Energy*, **217**, 179-18.

An, K.N., Himeno, H., Tsumura, H., Kawai, T., & Chao, E.Y.S. (1990). Pressure distribution on articular surfaces: application to joint stability evaluation. *Journal of Biomechanics*, **23**, 1013-1020.

Bei, Y. & Fregly, B. J. (2004). Multibody dynamic simulation of knee contact mechanics. *Medical Engineering & Physics* (submitted).

Bendjaballah, M.Z., Shirazi-Adl, A., & Zukor, D.J. (1995). Biomechanics of the human knee joint in compression: Reconstruction, mesh generation and Finite element analysis. *The Knee*, **2**, 69-79.

Bendjaballah, M.Z., Shirazi-Adl, A., & Zukor, D.J. (1997). Finite element analysis of human knee joint in varus-valgus. *Clinical Biomechanics*, **12**, 139-148.

Bendjaballah, M.Z., Shirazi-Adl, A., & Zukor, D.J. (1998). Biomechanical response of the passive human knee joint under anterior-posterior forces. *Clinical Biomechanics*, **13**, 625-633.

Blankevoort, L., Kuiper, J.H., Huiskes, R., & Grootenboer, H.J. (1991). Articular contact in a three-dimensional model of the knee. *Journal of Biomechanics*, **24**, 1019-1031.

Burman, J. & Gebart, B.R. (2001). Influence from numerical noise in the objective function for flow design optimization. *International Journal of Numerical Methods for Heat and Fluid Flow*, **11**, 6-19.

Chang, P.B., Williams, B.J., Santer, T.J., Notz, W.I., & Bartel, D.L. (1999). Robust optimization of total joint replacements incorporating environmental variables. *Journal of Biomechanical Engineering*, **121**, 304-310.

Cohen, Z.A., Henry, J.H., McCarthy, D.M., Mow, V.C., & Ateshian, G.A. (2003). Computer simulations of patellofemoral joint surgery. *The American Journal of Sports Medicine*, **31**, 87-98.

Dhaher, Y.Y. & Kahn, L.E. (2002). The effect of vastus medialis forces on patello-femoralcontact: a model-based study. *Journal of Biomechanical Engineering*, **124**, 758-767.

Donahue, T.L.H., Rashid, M.M., Jacobs, C.R., & Hull, M.L. (2002). A finite element model of the human knee joint for the study of tibio-femoral contact. *Journal of Biomechanical Engineering*, **124**, 273-280.

Donzelli, P. S., & Spilker, R. L. (1998). A contact finite element formulation for biological soft hydrated tissues. *Computer Methods in Applied Mechanics and Engineerin*, **153**, 63–79.

Donzelli, P.S., Spilker, R.L., Ateshian, G.A., & Mow, V.C. (1999). Contact analysis of biphasic transversely isotropic cartilage layers and correlations with tissue failure. *Journal of Biomechanics*, **32**, 1037-1047.

Fregly, B.J., Bei, Y., & Sylvester, M.E. (2003). Experimental evaluation of a multibody dynamic model to predict contact pressures in knee replacements. *Journal of Biomechanics*, **36**, 1658-1668.

Haider, M.A., & Guilak, F. (2000). Axisymmetric boundary integral model for incompressible linear viscoelasticity: Application to the micropipette aspiration contact problem. *Journal of Biomechanical Engineering*, **122**, 236-244.

Han, S.-K., Federico, S., Epstein, M., & Herzon, W. (2004). An articular cartilage contact model based on real surface geometry. *Journal of Biomechanics* (in press).

Harris, M.L., Morberg, P., Bruce, W.J.M., & Walsh, W.R. (1999). An improved method for measuring tibiofemoral contact areas in total knee arthroplasty: A comparison of K-scan sensor and Fuji film. *Journal of Biomechanics*, **32**, 951-958.

Hasler, E.M., Herzog, W., Wu, J.Z., Muller, W., & Wyss, U. (1998). Articular cartilage biomechanics: theoretical models, material properties, and biosynthetic response. *Critical Reviews in Biomedical Engineering*, 27, 415-488

Haut, T.L., Hull, M.L., Rashid, M.M., & Jacobs, C.R. (2002). A finite element model of the human knee joint for the study of tibio-femoral contact. *Journal of Biomechanical Engineering*, **124**, 273-280.

Herzog, W., Longino, D., & Clark, A. (2003). The role of muscles in joint adaptation anddegeneration. *Langenbeck's Archives of Surgery*, **388**, 305-315.

Holland, P.W., & Welsch, R.E. (1977). Robust regression using iteratively reweighted least-squares. *Communications in Statistics: Theory and Methods*, **6**, 813-827

Hong, J.H., Mun, M.S., & Song, S.H. (2001). An optimum design methodology development using a statistical technique for vehicle occupant safety. *Proceedings of the Institution of Mechanical Engineers, Part D: Journal of Automobile Engineering*, **215**, 795-801.

Hurwitz, D.E., Sumer, D.R., Andriacchi, T.P., & Sugar, D.A. (1998). Dynamic knee loads during gait predict proximal tibial bone distribution. *Journal of Biomechanics*, **31**, 423-430.

Jansson, T., Nilsson, L., & Redhe, M. (2003). Using surrogate models and response surfaces in structural optimization - With application to crashworthiness design and sheet metal forming. *Structural and Multidisciplinary Optimization*, **25**, 129-140.

Johnson, K.L. (1985). *Contact Mechanics.* Cambridge University Press, New York.

Jung, E.S. & Choe, J. (1996). Human reach posture prediction based on psychophysical discomfort. *International Journal of Industrial Ergonomics*, **18**, 173-179.

Jurvelin, J.S., Arokoski, J.P., Hunziker, E.B., & Helminen, H.J. (2000). Topographical variation of the elastic properties of articular cartilage in canine knee. *Journal of Biomechanics*, **33**, 669-75.

Kaufman, K.R., Kovacevic, N., Irby, S.E., & Colwell, C.W. (1996). Instrumented implant for measuring tibiofemoral forces. *Journal of Biomechanics*, **29**, 667-671.

Keane, A.J. (2003). Wing optimization using design of experiment, response surface, and data fusion methods. *Journal of Aircraft*, **40**, 741-750.

Komistek, R. D., Dennis, D. A., & Mahfouz, M. (2003). In vivo fluoroscopic analysis of the normal human knee. *Clinical Orthopaedics and Related Research*, **410**, 69-81.

Kuo, C.H. & Keer, L.M. (1993). Contact stress and fracture analysis of articular cartilage. *Biomedical Engineering Applications Basis Communications*, **5**, 515-521.

Kwak, S.D., Blankevoort, L., & Ateshian, G.A. (1999). A mathematical formulation for 3D quasi-static multibody models of diarthrodial joints. *Computer Methods in Biomedical Engineering*, **3**, 41-64.

Laasanen, M.S., Toyras, J., Korhonen, R.K., Rieppo, J., Saarakkala, S., Nieminen, M.T., Hirvonen, J., & Jurvelin, J.S. (2003). Biomechanical properties of knee articular cartilage, *Biorheology*, **40**, 133-140.

Leary, S.J., Bhaskar, A., & Keane A.J. (2004). Global approximation and optimization using adjoint computational fluid dynamics codes. *AIAA Journal*, **42**, 631-641.

Li, G., Sakamoto, M., & Chao, E.Y.S. (1997). A comparison of different methods in predicting static pressure distribution in articulating joints. *Journal of Biomechanics*, **30**, 635-638.

Li, G., Gil, J., Kanamori, A., & Woo, S.L.-Y. (1999). A validated 3D computational model of a human knee joint. *Journal of Biomechanical Engineering*, **121**, 657-662.

Li, G., Lopez, O., & Rubash, H. (2001). Variability of a 3D finite element model constructed using MR Images of a knee for joint contact stress analysis. *Journal of Biomechanical Engineering*, **123**, 341-346.

Liu, B., Haftka, R.T., & Akgun, M.A. (2000). Two-level composite wing structural optimization using response surfaces. *Structural and Multidisciplinary Optimization*, **20**, 87-96.

MacWilliams, B.A., DesJardins, J.D., Wilson, D.R., Romero, J., & Chao, E.Y.S. (1998). A repeatable alignment method and local coordinate description for knee joint testing and kinematic measurement. *Journal of Biomechanic*s, **31**, 947-950.

Mow, V.C., Kuei, S.C., Lai, W.M., & Armstrong, C.G. (1980). Biphasic creep and stress relaxation of articular cartilage in compression: Theory and experiments. *Journal of Biomechanical Engineering*, **102**, 73-84.

Mow, V.C., Lai, W.M., & Holmes, M.H. (1982). *Advanced theoretical and experimental techniques in cartilage research. In Biomechanics: Principles and Applications* (edited by R. Huiskes, D. van Campen, and J. DeVijn), Martinus Nijhoff Publishers, Boston, 63-69

Mukherjee, N. & Wayne, J.S. (1998). Load sharing between solid and fluid phases in articular cartilage: I--Experimental determination of in situ mechanical conditions in a porcine knee. *Journal of Biomechanical Engineering*, **120**, 614–619.

Otto, J.K., Brown, T.D., & Callaghan, J.J. (1999). Static and dynamic response of a multiplexed-array piezoresistive contact sensor. *Experimental Mechanics*, **39**, 317-323.

Pandy, M.G. & Sasaki, K. (1998). A three-dimensional musculoskeletal model of the human knee joint. Part 2: Analysis of ligament function. *Computer Methods in Biomechanics and Biomedical Engineering*, **1**, 265-283.

Papila, N., Shyy, W., Griffin, L., & Dorney, D.J. (2002). Shape optimization of supersonic turbines using global approximation methods. *Journal of Propulsion and Power*, **18**, 509-518.

Périé, D. & Hobatho, M.C. (1998). In vivo determination of contact areas and pressure of the femorotibial joint using non-linear finite element analysis. *Clinical Biomechanics*, **13**, 394-402.

Piazza, S.J. & Delp, S.L. (2001). Three-dimensional dynamic simulation of total knee replacement motion during a step-up task. *Journal of Biomechanical Engineering*, **123**, 599-606.

Rikards, R., Abramovich, H., Auzins, J., Korjakins, A., Ozolinsh, O., Kalnins, K., & Green, T. (2004). Surrogate models for optimum design of stiffened composite shells. *Composite Structures*, **63**, 243-251.

Roux, W.J., Stander, N., & Haftka, R.T. (1998). Response surface approximations for structural optimization. *International Journal for Numerical Methods in Engineering*, **42**, 517-534.

Sevant, N.E., Bloor, M.I.G., & Wilson, M.J. (2000). Aerodynamic design of a flying wing using response surface methodology. *Journal of Aircraft*, **37**, 562-569.

Schipplein, O.D. & Andriacchi, T.P. (1991). Interaction between active and passive knee stabilizers during level walking. *Journal of Orthopaedic Research*, **9**, 113-119.

Setton, L.A., Elliot, D.M., & Mow, V.C. (1999). Altered mechanics of cartilage with osteoarthritis: human osteoarthritis and an experimental model of joint degeneration. *Osteoarthritis and Cartilage*, **7**, 2-14.

Shepherd, D.E.T. & Seedhom B.B. (1997). A technique for measuring the compressive modulus of articular cartilage under physiological loading rates with preliminary results. *Journal of Engineering in Medicine*, **211**, 155-165.

Stolk, J., Verdonschot, N., Cristofolini, L., Toni, A., & Huiskes, R. (2002). Finite element and experimental models of cemented hip joint reconstructions can produce similar bone and cement strains in pre-clinical tests. *Journal of Biomechanics*, **35**, 499-510.

Tashman, S. & Anderst, W. (2003). In-vivo measurement of dynamic joint motion using high speed biplane radiography and CTL: application to canine ACL deficiency. *Journal of Biomechanical Engineering*, **125**, 238-245.

Wu, J.Z., Herzog, W., & Epstein, M. (1998). Effects of inserting a pressensor film into articular joints on the actual contact mechanics. *Journal of Biomechanical Engineering*, **120**, 655-659.

BIOGRAPHICAL SKETCH

Yi-Chung Lin was born on August 14, 1976, in Kaohsiung, Taiwan. In 1998, he received the bachelor's degree in the Department of Mechanical Engineering of the National Cheng Kung University, Taiwan. He joined the Computational and Biomechanics Laboratory of Assistant Professor B. J. Fregly in the fall of 2002. He is planning to enter the doctoral program in mechanical and aerospace engineering after finishing the master's program.